



ACCEPTED MANUSCRIPT

This is an early electronic version of an as-received manuscript that has been accepted for publication in the Journal of the Serbian Chemical Society but has not yet been subjected to the editing process and publishing procedure applied by the JSCS Editorial Office.

Please cite this article as: N. B. Nguyen, T. Q. P. Phan, C. T. T. Pham, H. N. Nguyen, S. N. Pham, Q. K. A. Nguyen, D. T. Nguyen, *J. Serb. Chem. Soc.* (2022) <https://doi.org/10.2298/JSC220802080N>

This “raw” version of the manuscript is being provided to the authors and readers for their technical service. It must be stressed that the manuscript still has to be subjected to copyediting, typesetting, English grammar and syntax corrections, professional editing and authors’ review of the galley proof before it is published in its final form. Please note that during these publishing processes, many errors may emerge which could affect the final content of the manuscript and all legal disclaimers applied according to the policies of the Journal.



J. Serb. Chem. Soc. **00(0)** 1-12 (2022)
JSCS-12026

Performance of carbon-coated magnetic nanocomposite in methylene blue and arsenate treatment from aqueous solution

NGOC BICH NGUYEN^{1,2*}, THI QUE PHUONG PHAN³, CAO THANH TUNG PHAM^{1,4},
HUU NGHI NGUYEN², SY NGUYEN PHAM⁵, QUOC KHUONG ANH NGUYEN^{6**} and
DINH THANH NGUYEN^{1,3***}

¹Graduate University of Science and Technology, Viet Nam Academy of Science and Technology, Hanoi City, 100000, Vietnam; ²Dong Thap University, Cao Lanh City, 870000, Vietnam; ³Institute of Applied Materials Science, Viet Nam Academy of Science and Technology, Ho Chi Minh City, 700000, Vietnam; ⁴Institute of Chemical Technology, Viet Nam Academy of Science and Technology, Ho Chi Minh City, 700000, Vietnam; ⁵Ho Chi Minh City University of Natural Resources and Environment, Vietnam and ⁶Institute of Applied Technology and Sustainable Development, Nguyen Tat Thanh University, Ho Chi Minh City, 70000, Vietnam

(Received 2 August; Revised 5 October; Accepted 3 November 2022)

Abstract: Herein, carbon-coated magnetic nanocomposite fabricated by a low-temperature hydrothermal method was used for methylene blue and arsenate treatment in aqueous solution. The Langmuir model fits the experimental data with a calculated maximum adsorption capacity of 110.63 and 2.31 mg g⁻¹ for methylene blue and arsenate adsorption, respectively. Furthermore, the adsorption mechanisms of methylene blue as well as arsenate are physical adsorption and a combination of physical adsorption and chemisorption, respectively. Gibbs free energy change with negative values indicates that methylene blue and arsenate adsorption on magnetic materials occurs naturally. This research demonstrated a simple, efficient, and reliable method for removing methylene blue and arsenate.

Keywords: hydrothermal carbonization; rice straw; adsorption

INTRODUCTION

The rapid development of industries has posed many potentially serious issues in relation to ecosystems such as heavy metal and dye contamination.¹ Several technologies have been introduced for wastewater treatment, including oxidation, photocatalytic degradation, ultrafiltration, adsorption/precipitation process, and coagulation.² Adsorption has been regarded as one of the most common and effective techniques for contaminant removal from wastewater.³ Recently, carbon material derived from low-cost biomass residuals such as rice straw has received

Corresponding authors E-mail: (*)nbich@dthu.edu.vn; (**)nqkanh@ntt.edu.vn;
(***)dinhthanhg53@gmail.com
<https://doi.org/10.2298/JSC220802080N>

a lot of attention due to its potential environmental benefits.⁴ Moreover, magnetic modifications of the low-cost adsorbents can result in novel adsorbents that can be rapidly removed from the treated solution using a magnetic separator.⁵

Methylene blue (MB) is used in many fields, so a significant amount of MB ends up in wastewater, posing a risk to aquatic life. In addition, due to its high toxicity, arsenic can cause serious health problems such as lung, liver, kidney, and skin cancers.⁶⁻¹¹ As a result, it is critical to investigate efficient technologies for extracting MB and As(V) from aqueous solutions.¹²⁻¹⁶ Rice straw (RS) is an inexpensive and abundant carbon-containing lignocellulose in Vietnam. In the paper industry, biomass is usually pre-alkali-treated to remove lignin. As a result, this process emits a large amount of black liquor containing lignin, which can be utilized for carbon-containing materials.¹⁷

In this study, we simultaneously carbonize and magnetize the lignin liquor obtained from rice straw to synthesize carbon-coated magnetic nanocomposite (CMC) by a hydrothermal method. The primary goal of this work is to study the potential adsorption of low-cost CMC for MB and As(V) from wastewater. Aside from that, another goal is to evaluate the effect of concentration, contact time, temperature, and pH solution. This work also discusses the Langmuir and Freundlich adsorption isotherm models, as well as various thermodynamic parameters like heat of adsorption (ΔH°), entropy change (ΔS°), and Gibbs free energy change (ΔG°) in MB and As(V) adsorption.

EXPERIMENTAL

Materials

RS was collected in Vietnam and washed several times with distilled water before being milled into powder and filtered through a 250 - mesh sieve.

Potassium hydroxide (KOH, $\geq 85\%$), sodium hydroxide (NaOH, $\geq 97\%$), hydrochloric acid (HCl, 37%), iron (III) nitrate nonahydrate ($\text{Fe}(\text{NO}_3)_3 \cdot 9\text{H}_2\text{O}$, $\geq 99\%$), sodium chloride (NaCl, $\geq 99.5\%$), H_3AsO_4 in HNO_3 0.5 mol L⁻¹ 1000 mg L⁻¹ purchased from Merck. MB ($\text{C}_{16}\text{H}_{18}\text{N}_3\text{SCl}_x\text{H}_2\text{O}$, 99.5%), was obtained from Sigma - Aldrich. All chemicals used were of analytical grade and were used as received without any further purification.

Synthesis of carbon-coated magnetic nanocomposite

Firstly, 15 g of RS was combined with 150 ml KOH 5%. The mixture was hydrothermally treated in an autoclave at 120 °C for 4 h. After slowly mixing 50 ml of 0.125 mol $\text{Fe}(\text{NO}_3)_3$ into 125 ml of the above-solution for 2 h, hydrothermal treatment was carried out at 180 °C for 14 h. The CMC is then collected by filtration and washed several washes with distilled water until the pH value reached neutral. Finally, the remaining solid was dried in an oven at 40 °C for 12 h. In comparison, a blank sample (BS) was fabricated under the same condition but without the addition of $\text{Fe}(\text{NO}_3)_3$.

Characterization of CMC

X-ray diffraction (XRD) was carried out ON X D8 Advance - Bruker with Cu K_α radiation ($\lambda = 0,15418$ nm). The morphology was observed with S4800 - Hitachi scanning electron microscope (SEM) and JEM1400 - JEOL transmission electron microscopy (TEM). Energy-

dispersive X-ray spectrum (EDS) was recorded on H7593 - Horiba. The Fourier transform infrared (FT-IR) spectroscopy was measured on IR Affinity-1S spectrophotometer (Shimadzu). The specific surface area (BET) was determined by N₂ adsorption-desorption isotherms at liquid nitrogen temperature (77 K) using Quantachrome TriStar 3000 V6.07A adsorption instruments. Magnetization measurements were carried out using a vibrating sample magnetometer (VSM) 7307, Lake Shore, USA. The UV-Vis spectrometry was recorded on Spectro UV-2650, Labomed, USA, at a wavelength of 664 nm. Residual As(V) was detected by Thermo Scientific iCAP Q ICP-MS. The point of zero charge (pH_{PZC}) of CMC was investigated by the solid addition method.¹⁸ A series of 45 mL of 0.5 M NaCl solutions were prepared in 100 mL flasks. The initial pH value (pH_i) of the solution was adjusted from 2 to 12 using either 0.1 M NaOH or 0.1 M HCl solutions. The total volume of solution in each flask was precisely 50 mL by adding distilled water. Then, 0.1 g of CMC was added to each flask and kept on shaker at 180 rpm for 24 h. The final pH (pH_f) of the solutions was recorded. The difference between the initial and final pH ($\Delta\text{pH} = \text{pH}_i - \text{pH}_f$) was plotted against pH_i. The point of intersection of the curve with the abscissa, where $\Delta\text{pH} = 0$, presented pH_{PZC}.

Adsorption experiment

Adsorption experiments were carried out using 0.1 g CMC in 100 mL of solution. Variable parameters including initial concentration, contact time, temperature, and pH of the medium were thoroughly investigated. The initial pH value of the solution was adjusted using either 0.1 M NaOH or 0.1 M HCl solutions. All adsorption experiments were carried out in duplicate. At predetermined time intervals, the adsorbent and solution were separated, and the residual MB and As(V) concentrations in the solution were measured using UV - VIS and ICP - MS, respectively.

The removal rate, R / % were calculated using equation (1):

$$R = \frac{C_0 - C_e}{C_0} \times 100 \quad (1)$$

where C_0 and C_e are the initial and equilibrium concentrations of MB or As(V) solution. We listed different kinetic models, thermodynamic equations, and adsorption isotherms in Table S-I.

Non-linear Chi-square test

Optimization is indispensable in order to identify the suitable kinetic and isotherm models to the obtained experimental results. For the present study, apart from correlation coefficient (R^2), a non-linear regression model is chi-square test was performed for data optimization process. The chi-square (χ^2) can be expressed as equation (2):

$$\chi^2 = \sum \frac{(q_{e,\text{exp}} - q_{e,\text{cal}})^2}{q_{e,\text{cal}}} \quad (2)$$

where $q_{e,\text{exp}}$ is the experimental value of adsorption capacity and $q_{e,\text{cal}}$ is the calculated value from the model. If experimental data is analogous to that from the model, χ^2 will be small, otherwise, it will be large.

Reusability

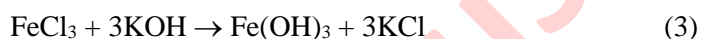
0.1 g CMC was added to 100 mL of a solution (120 mg L⁻¹ for MB and 2.5 mg L⁻¹ for As(V) and stirred for 60 and 90 min, respectively, for saturated adsorption. Following the magnetic separation, the supernatant solution was discarded, and only adsorbed CMC was

collected. The adsorbed CMC in the case of MB was then added to ethanol and a 0.1 M HCl solution in the case of As(V) for the desorption process.¹³⁻¹⁴ The experiments were repeated 5 times in sequence to estimate the potentially regenerable property of CMC.

RESULTS AND DISCUSSION

Characterization of materials

As shown in Fig. 1a, regarding BS, the broad peak at $2\theta = 22^\circ$ represented the characteristic reflection of carbon.¹⁹ In CMC, the diffractions at $2\theta = 30.46; 35.86; 43.58; 57.25$ and 62.65° correspond to crystalline magnetite Fe_3O_4 (JCPDS No. 19-0629), which agree with the literature data.²⁰ This demonstrated that Fe(III) is reduced into Fe_3O_4 by carbon, which is formed under hydrothermal conditions by the reactions (3-6).²



In Fig. 1b, FT-IR spectra revealed that both BS and CMC contained functional groups at $3413\text{-}3422\text{ cm}^{-1}$ (-OH stretching vibrations), $1627\text{-}1630\text{ cm}^{-1}$ (C=O stretching vibration), $1110\text{-}1114\text{ cm}^{-1}$ (C-O stretching vibration), $799\text{-}818\text{ cm}^{-1}$ and $450\text{-}474\text{ cm}^{-1}$ (Si-O-Si stretching vibration) and $1451\text{-}1456\text{ cm}^{-1}$ (-O-CH₃ deformation vibration).^{1,18, 20} In general, the intensity of all peaks in CMC is lower than that of BS and has a slight shift, indicating that chemical reactions occurred when Fe^{3+} was added to the solution. The peak near 560 cm^{-1} , assigned to the Fe-O stretching vibration, was only visible in CMC, which is consistent with XRD result.¹²

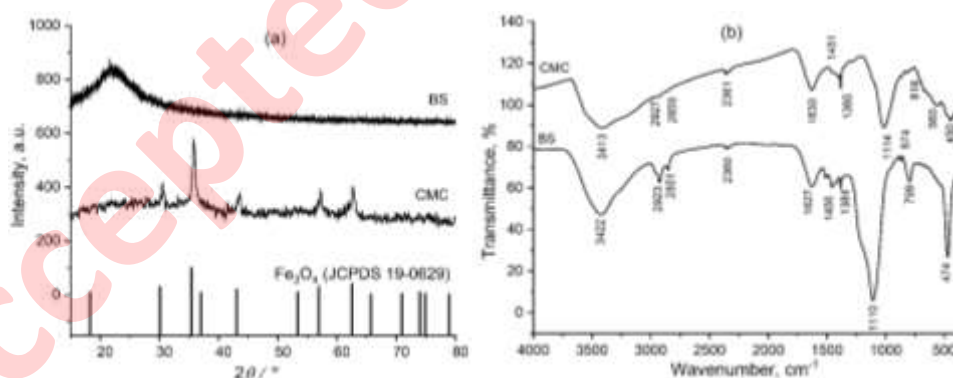


Fig. 1. a) XRD patterns of BS, CMC, and standard Fe_3O_4 (JCPDS No. 19-0629) b) FT-IR spectra of BS and CMC

According to Figures S-1 and S-2, CMC is made up of C (19.21 %), O (34.38 %), Fe (42.24 %) and Si (4.16 %). In addition, EDS elemental mapping also shows that Fe is uniformly dispersed on the surface of the material, proving that

iron oxide was formed in CMC. Fig. 2a and 2b depicts typical TEM and SEM images of CMC containing Fe_3O_4 with sizes ranging from 50 to 120 nm and carbon as a shell with a thickness ranging from 30 to 50 nm. At room temperature, Fig. S-3 shows the saturation magnetisation value of 33.7 emu g^{-1} , which allows for the rapid separation and redistribution of CMC from aqueous solution and leads to cost-effective and reusable applications.²¹ Table S-II compares the magnetization of CMC with various biochar.

Table S-III displayed specific surface area, total pore volume, and mean pore size for RS, BS, and CMC. The specific surface area of CMC ($171.4 \text{ m}^2 \text{ g}^{-1}$) is significantly greater than that of BS ($6.6 \text{ m}^2 \text{ g}^{-1}$) thanks to the combination of carbon and magnetic particles.²² Furthermore, the mean pore size of CMC (6 nm) is smaller than that of BS (33 nm), attributed to the covered micropores in carbon.²³

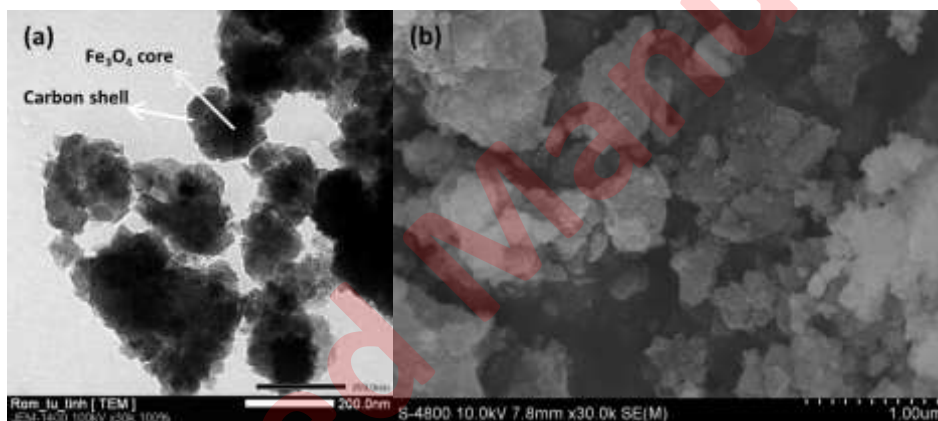


Fig. 2. TEM (a) and SEM (b) images of CMC

Effect of initial solution pH

The pH of the solution plays an important role in the adsorption process, particularly in terms of adsorption capacity.²⁴ Because of the changing surface of CMC on MB and As(V), the pH value can alter its performance.²⁵ Investigating the influence of initial pH solutions from 3 to 11 was carried out while keeping other parameters constant such as initial concentration (120 and 2.5 mg L^{-1}), equilibrium time (60 and 90 min at 303 K) for MB and As(V), respectively. The effect of pH on the adsorption of MB and As(V) on CMC is depicted in Fig. 3a and 3b.

The adsorption capacity of MB increases from 3 to 7 and changes slightly when solution pH exceeds 7. When $\text{pH} < \text{pH}_{\text{PZC}}$, the surface charge is positive, and when $\text{pH} > \text{pH}_{\text{PZC}}$, the surface charge is negative. The pH_{PZC} of CMC is approximately 6.32 (Fig. S-4).

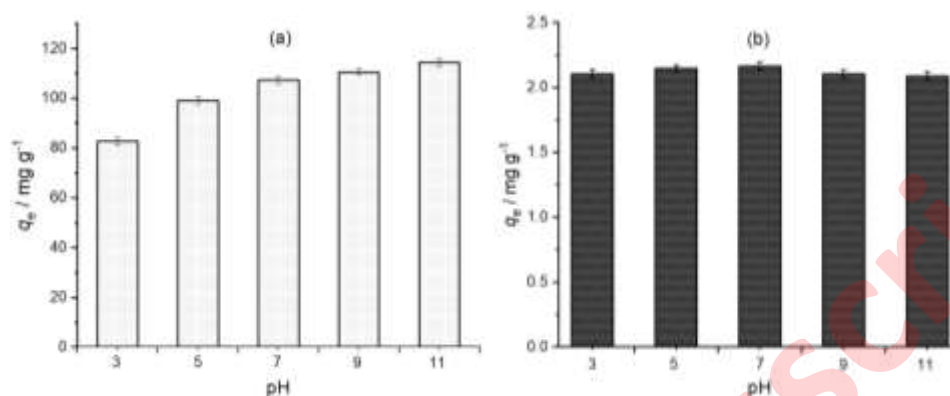


Fig. 3. Influence of pH value on the adsorption of (a) MB and (b) As(V)

At low pH, low adsorption capacity resulted from electrostatic repulsion between the cationic ion MB and positively charged active sites on CMC. Electrostatic attraction occurs between negatively active sites on CMC and the cationic ion MB at higher pH levels, facilitating adsorption capacity. Arsenic acid exists in anionic forms (H_2AsO_4^- , HAsO_4^{2-} , AsO_4^{3-}).²⁶ Moreover, CMC with positively charged active sites can attract arsenate ions, increasing adsorption capacity from 84.12 to 86.6 %. In contrast, at pH ranging 7 to 11, CMC with negatively charged active sites inhibited As(V) adsorption due to OH^- competing with arsenate ions, resulting in a decrease in yield to 83.54 %.²⁷ Hence, the initial pH solution for the following experiments is 7.

Adsorption thermodynamics

A linear van't Hoff plot (Fig. 4a and 4b) of $\ln K_D$ versus $1/T$ gives slope and intercept to determine the value of ΔH° and ΔS° , respectively. The calculated thermodynamic parameters for MB and As(V) adsorption onto CMC are summarized in Table I at different temperatures. As temperature rises, the value of ΔG° becomes more negative, resulting in more spontaneous adsorption with high affinity of MB and As(V) to CMC. The value of ΔH° for absolute physical adsorption is typically less than 20 kJ mol^{-1} , whereas chemisorption is in the range of 80 to 200 kJ mol^{-1} .^{28, 29}

TABLE I. Thermodynamic parameters for adsorption of adsorbates onto CMC

Adsorbate	Temperature, K	$\Delta S^\circ / \text{J mol}^{-1} \text{K}^{-1}$	$\Delta H^\circ / \text{kJ mol}^{-1}$	$\Delta G^\circ / \text{kJ mol}^{-1}$
MB	303	67.41	15.06	-5.38
	313			-6.01
	323			-6.73
As	303	89.10	22.32	-4.70
	313			-5.51
	323			-6.49

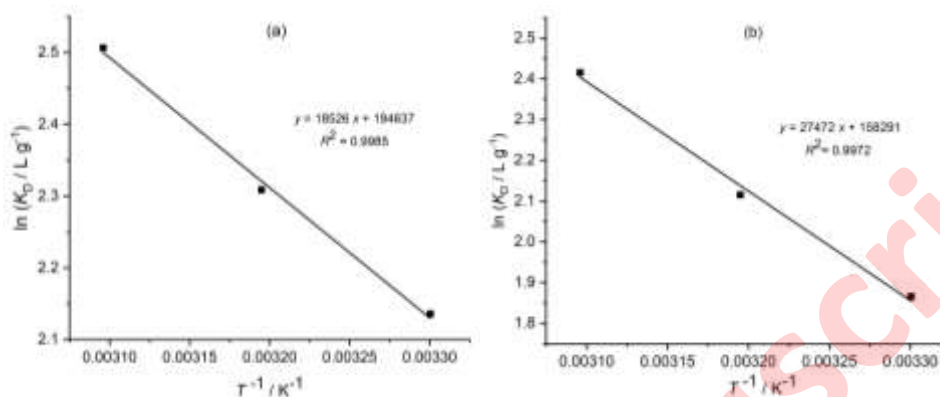


Fig. 4. The plot of $\ln K_D$ vs. $1/T$ for a) MB and b) As(V) adsorption onto CMC

ΔH° of MB on CMC is $15.06 \text{ kJ mol}^{-1}$ indicates physical adsorption while the value of ΔH° ($22.32 \text{ kJ mol}^{-1}$) for As(V) on CMC should be regarded as a mixture of physical adsorption and chemisorption, but dominated by physical adsorption, since the ΔH° was a slightly higher than 20 kJ mol^{-1} . With positive values of ΔS° , there is an affinity adsorbent for adsorbate.

Effect of contact time and adsorption kinetics

For both MB and As(V), contact intervals of 0 to 105 min and 0 to 120 min are used to evaluate the adsorption process as a function of contact time, respectively. The adsorption of MB and As(V) occurs in three stages. Firstly, the adsorption rate for MB increases significantly in 10 min and 30 mins for As(V). The reason for this is that at the start, many vacant sites are available for adsorption. Then, it will gradually rise until it reaches the equilibrium value of 30 min for MB and 75 min for As(V) (Fig. 5a and 5b), resulting from the fewer vacant sites and repulsive forces between the occupied sites and bulk phases.

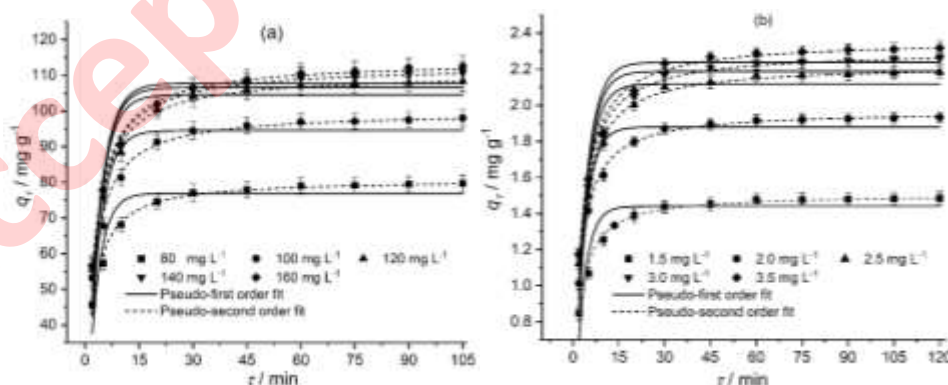


Fig. 5. Kinetic modeling for adsorption of a) MB and b) As(V) onto CMC

Therefore, we determined that the adsorption time for the next experiment will be 60 min for MB and 90 min for As(V). Adsorption of MB on the surface of CMC is physical whereas adsorption of As(V) is both physical and chemical, resulting in As(V) adsorption being slower than that of MB.^{30, 31}

To investigate the experimental data, different kinetic models including pseudo-first-order and pseudo-second-order were used to understand the adsorption process. The kinetic parameters, correlation coefficient (R^2) and non-linear Chi-square (χ^2) were listed in Table II.

The calculated q_e values ($q_{e,cal}$) of both models are comparable to the experimental ones ($q_{e,exp}$). However, the R^2 of the pseudo-second-order kinetic model (approximately 0.99 for R^2) is significantly higher than that of pseudo-first-order kinetic model (approximately 0.90 for R^2), conversely, (χ^2) of the pseudo-second-order kinetic model is significantly lower than that of pseudo-first-order kinetic model, implying that the pseudo-second-order kinetic model is better for adsorption kinetics of MB and As(V) onto CMC.

TABLE II. Kinetic parameters for adsorption of a) MB; b) As(V) onto CMC at 303 K

Adsorbate	$C_0 /$ mg L^{-1}	First-order kinetic model					Second-order kinetic model				
		$q_{e,exp} /$ mg g^{-1}	$k_1 /$ min^{-1}	$q_{e,cal} /$ mg g^{-1}	R^2	χ^2	$k_2 /$ $\text{g mg}^{-1} \text{min}^{-1}$	$q_{e,cal} /$ mg g^{-1}	R^2	χ^2	
MB	80	79.74	0.3357	76.94	0.864	3.043	0.0071	80.87	0.987	0.274	
	100	98.03	0.2972	94.56	0.875	4.403	0.0050	99.72	0.986	0.459	
	120	108.35	0.2870	104.55	0.900	3.950	0.0042	110.51	0.994	0.207	
	140	110.91	0.2830	106.58	0.899	4.120	0.0041	112.78	0.995	0.193	
	160	112.57	0.2796	107.75	0.893	4.473	0.0039	114.12	0.994	0.244	
As(V)	1.5	1.482	0.3325	1.442	0.867	0.059	0.3774	1.507	0.987	0.006	
	2.0	1.929	0.3084	1.880	0.915	0.053	0.2608	1.971	0.998	0.001	
	2.5	2.179	0.2784	2.119	0.902	0.089	0.2049	2.227	0.993	0.006	
	3.0	2.257	0.2752	2.189	0.888	0.104	0.1961	2.302	0.991	0.009	
	3.5	2.312	0.2713	2.239	0.886	0.108	0.1855	2.362	0.989	0.010	

Effect of initial concentration and adsorption isotherms

Fig. 6a and 6b indicated that the adsorption capacity of MB and As(V) onto CMC significantly increases with increasing ranges of 80 to 120 mg L^{-1} and 1.5 to 2.5 mg L^{-1} , respectively. When the concentrations of MB and As(V) exceed 120 and 2.5 mg L^{-1} , the adsorption capacity increases insignificantly and reaches a maximum of 110.63 mg L^{-1} ($C_0 = 160 \text{ mg L}^{-1}$) and 2.312 mg L^{-1} ($C_0 = 3.5 \text{ mg L}^{-1}$), respectively. We can assume three main reasons to explain this phenomenon 1) a large number of available active sites are used at higher concentrations of MB and As(V) 2) improved mass transfer 3) the increased ability of MB and As(V) to collide with CMC.

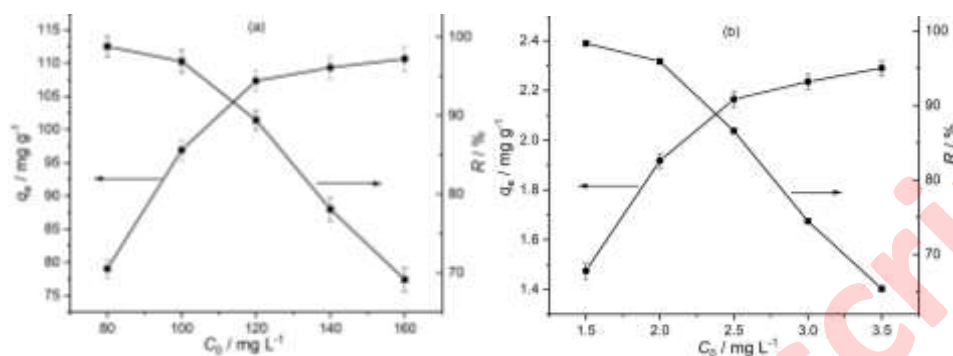


Fig 6. Effect of initial concentration on adsorption capacity and removal efficiency of a) MB and b) As(V) onto CMC

Furthermore, as the initial concentration increases from 80 to 160 mg L⁻¹ and from 1.5 to 3.5 mg L⁻¹, the removal of MB and As(V) decreases from 98.79 to 69.14 % and 98.60 to 65.97 %, respectively. When using higher concentrations of adsorbates with the same weight of CMC, the percentage removal of MB and As(V) is reduced because the number of active sites on CMC remains constant.

The Langmuir and Freundlich equations are the most used isotherms equation for modelling the adsorption data. The R^2 obtained from Langmuir model is significantly higher than that obtained from Freundlich model, indicating that the Langmuir isotherm better fits the experimental data (Fig. 7a and 7b, Table III). Table S-IV compares the adsorption capacity of CMC with various adsorbents. The previously reported capacity of MB and As(V) onto CMC is greater than that of many other previously reported adsorbents, implying that the as-prepared CMC has a high potential for use in wastewater treatment. A high K_L value indicates the high affinity of adsorbent for MB and As(V) adsorption.^{32, 33} The R_L values in the range of 0 and 1 indicate favourable adsorption.

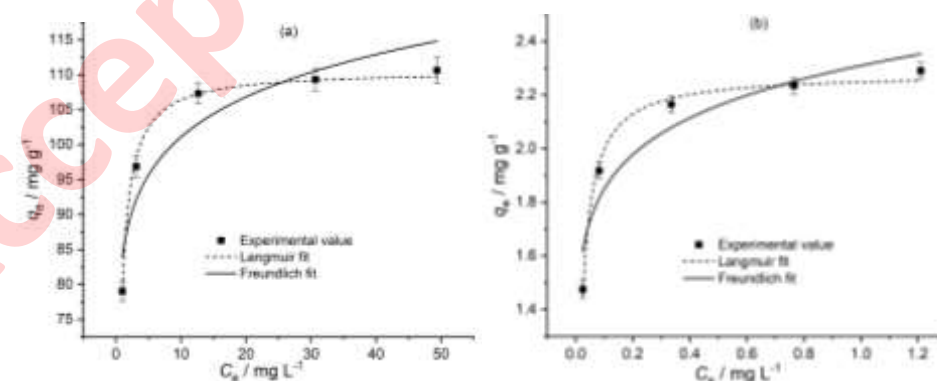


Fig. 7. Analyses of adsorption isotherm for a) MB and b) As(V) onto CMC by Langmuir and Freundlich models at 303 K

TABLE III. Isotherm parameters for adsorption of MB and As(V) onto CMC at different concentration

Adsorbate	$q_{e,exp} / \text{mg g}^{-1}$	Langmuir isotherm model				Freundlich isotherm model				
		$q_{max} / \text{mg g}^{-1}$	$K_L / \text{L mg}^{-1}$	R_L	R^2	χ^2	$K_F / \text{mg g (L/mg)}^{1/n}$	n_F	R^2	χ^2
MB	110.63	110.64	2.518	0.0030	0.9960	0.027	84.138	12.546	0.884	24.427
As(V)	2.31	2.285	81.919	0.0030	0.9850	0.003	2.325	10.950	0.904	0.608

Reusability

CMC regeneration and recycling are critical for practical application. As shown in Fig. 8a and 8b, after five cycles, there is only a very slight decrease in removal from 107.32 to 98.73 mg g^{-1} for MB and from 2.165 to 1.992 mg g^{-1} for As(V), indicating that CMC has excellent performance and application for MB and As (V) treatment.

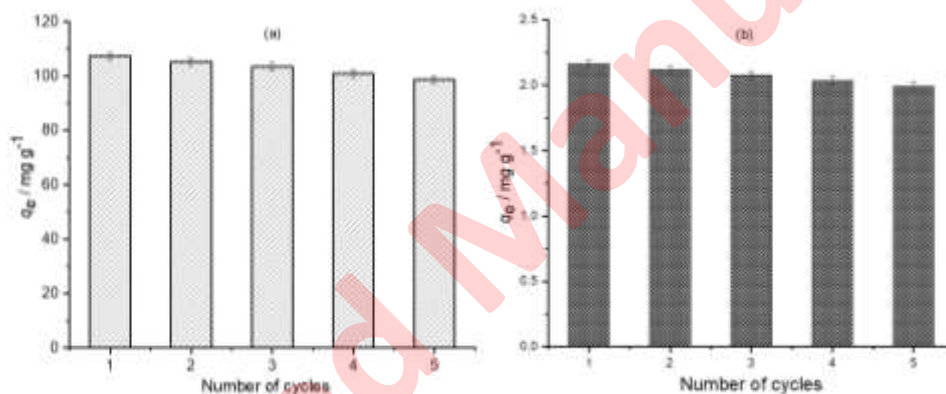


Fig. 8. Regeneration for (a) MB and (b) As(V) adsorption onto CMC

CONCLUSION

CMC was prepared in a straightforward and efficient manner. They also have a fast adsorption rate, high adsorption efficiency, and fast magnetic separation from treated water, making them excellent materials for environmentally treated purposes. The maximum adsorption is 110.63 mg g^{-1} for MB and 2.31 mg g^{-1} for As(V). The kinetics of adsorption can be described using a pseudo-second-order equation, and the CMC adsorption isotherm agreed well with the Langmuir sorption equation. Furthermore, through the desorption process, the product could be regenerated and reused multiple times.

SUPPLEMENTARY MATERIAL

Additional data are available electronically at the pages of journal website: <https://www.shd-pub.org.rs/index.php/JSCS/article/view/12026>, or from the corresponding author on request.

ИЗВОД

КАРАКТЕРИЗАЦИЈА МАГНЕТНОГ НАНОКОМПОЗИТА ПРЕВУЧЕНОГ УГЉЕНИКОМ ЗА УКЛАЊАЊЕ МЕТИЛЕНСКО ПЛАВОГ И АРСЕНАТА ИЗ ВОДЕНОГ РАСТВОРА

NGOC BICH NGUYEN^{1,2}, THI QUE PHUONG PHAN³, CAO THANH TUNG PHAM^{1,4}, HUU NGHI NGUYEN², SY NGUYEN PHAM⁵ и DINH THANH NGUYEN^{1,3}

¹Graduate University of Science and Technology, Viet Nam Academy of Science and Technology, Hanoi City, 100000, Vietnam; ²Dong Thap University, Cao Lanh City, 870000, Vietnam; ³Institute of Applied Materials Science, Viet Nam Academy of Science and Technology, Ho Chi Minh City, 700000, Vietnam; ⁴Institute of Chemical Technology, Viet Nam Academy of Science and Technology, Ho Chi Minh City, 700000, Vietnam и ⁵Ho Chi Minh City University of Natural Resources and Environment, Vietnam

Магнетни наноконтролит превучен угљеником произведен ниско-температурском хидротермалном методом је употребљен за уклањање метиленско плавог и арсената из воденог раствора. Лангмиров модел је добро описао експерименталне податке са израчунатим максималним адсорпционом капацитетом од 110,63 и 2,31 mg g⁻¹ за метиленско плаво и арсенат, респективно. Такође, одређени адсорпциони механизми су физисорпција за метиленско плаво и комбинација физисорпције и хемисорпције за арсенат. Промена Гибсове слободне енергије има негативне вредности што указује да се адсорпција метиленско плавог и арсената на магнетним материјалима дешава спонтано. Ово истраживање показује једноставну, ефикасну и поуздану методу за уклањање метиленско плавог и арсената.

(Примљено 2. августа; ревидирано 5. октобра; прихваћено 3. новембра 2022.)

REFERENCES

1. S. Ji, C. Miao, H. Liu, L. Feng, X. Yang, H. Guo, *Nanoscale Res. Lett.* **13** (2018) 178 (<https://doi.org/10.1186/s11671-018-2580-8>)
2. W. J. Liu, K. Tian, H. Jiang, H. Q. Yu, *Sci Rep* **3** (2013) 2419 (<https://doi.org/10.1080/19443994.2015.1132476>)
3. T. H. Nguyen, T. H. Pham, H. T. N. Thi, T. N. Nguyen, M. V. Nguyen, T. T. Dinh, M. P. Nguyen, T. Q. Do, T. Phuong, T. T. Hoang, T. T. M. Hung, V. H. T. Thi, *J. Chem.* **2019** (2019) 1 (<https://doi.org/10.1155/2019/5295610>)
4. M. Inyang, B. Gao, P. Pullammanappallil, W. Ding, A. R. Zimmerman, *Bioresour. Technol.* **101** (2010) 8868 (<https://doi.org/10.1016/j.biortech.2010.06.088>)
5. N. Besharati, N. Alizadeh, S. Shariati, *J. Mex. Chem. Soc.* **62** (2018) 110 (<https://doi.org/10.29356/jmcs.v62i3.433>)
6. W. Chen, R. Parette, J. Zou, F. Cannon, B. Dempsey, *Water Res.* **41** (2007) 1851 (<https://doi.org/10.1016/j.watres.2007.01.052>)
7. M. Zhang, B. Gao, S. Varnoozfaderani, A. Hebard, Y. Yao, M. Inyang, *Bioresour. Technol.* **130** (2013) 457 (<https://doi.org/10.1016/j.biortech.2012.11.132>)
8. L. Huang, J. Cai, M. He, B. Chen, B. Hu, *Ind. Eng. Chem. Res.* **57** (2018) 6201 (<https://doi.org/10.1021/acs.iecr.7b05294>)
9. N. S. Pham, P. T. Q. Phan, B. N. Nguyen, V. X. Le, *J. Appl. Electrochem.* (2022) (<https://doi.org/10.1007/s10800-022-01747-1>)
10. N. S. Pham, V. X. Le, *J. Electroanal. Chem.* **921** (2022) 116507 (<https://doi.org/10.1016/j.jelechem.2022.116507>)
11. N. S. Pham, B. N. Nguyen, A. Q. K. Nguyen, *J. Appl. Electrochem.* (2022) (<https://doi.org/10.1007/s10800-022-01784-w>)

12. K. Dai, F. Wang, W. Jiang, Y. Chen, J. Mao, J. Bao, *Nanoscale Res. Lett.* **12** (2017) 528 (<https://doi.org/10.1186/s11671-017-2295-2>)
13. N. S. Pham, Y. H. Seo, E. Park, T. D. D. Nguyen, I.-S. Shin, *Data Br.* **31** (2020) 105891 (<https://doi.org/10.1016/j.dib.2020.105891>)
14. N. S. Pham, Y. H. Seo, E. Park, T. D. D. Nguyen, I.-S. Shin, *Electrochim. Acta* **353** (2020) 136446 (<https://doi.org/10.1016/j.electacta.2020.136446>)
15. V. X. Le, H. Lee, N. S. Pham, S. Bong, H. Oh, S.-H. Cho, I.-S. Shin, *Sens. Actuators B* **346** (2021) 130552 (<https://doi.org/10.1016/j.snb.2021.130552>)
16. N. S. Pham, P. T. Q. Phan, V. X. Le, *J. Appl. Electrochem.* **52** (2022) 1343 (<https://doi.org/10.1007/s10800-022-01716-8>)
17. L. Zhu, F. Shen, R. L. Smith, L. Yan, L. Li, X. Qi, *Chem. Eng. J.* **316** (2017) 770 (<https://doi.org/10.1016/j.cej.2017.02.034>)
18. L. Ai, C. Zhang, Z. Chen, *J. Hazard Mater.* **192** (2011) 1515 (<https://doi.org/10.1016/j.jhazmat.2011.10.041>)
19. X. Bao, Z. Qiang, J.-H. Chang, W. Ben, J. Qu, *J. Environ. Sci.* **26** (2014) 962 ([https://doi.org/10.1016/S1001-0742\(13\)60485-4](https://doi.org/10.1016/S1001-0742(13)60485-4))
20. L. Verma, M. A. Siddique, J. Singh, R. N. Bharagava, *J. Environ. Manage.* **250** (2019) 109452 (<https://doi.org/10.1016/j.jenvman.2019.109452>)
21. J. Wang, J. Xu, N. Wu, *J. Exp. Nanosci.* **12** (2017) 297 (<https://doi.org/10.1080/17458080.2017.1325016>)
22. B. Qiu, H. Gu, X. Yan, J. Guo, Y. Wang, D. Sun, Q. Wang, M. Khan, X. Zhang, B. L. Weeks, D. P. Young, Z. Guo, S. Wei, *J. Mater. Chem. A* **2** (2014) 17454 (<https://doi.org/10.1039/C4TA04040F>)
23. H. Zeng, W. Qi, L. Zhai, F. Wang, J. Zhang, D. Li, *J. Environ. Chem. Eng.* **9** (2021) 105951 (<https://doi.org/10.1016/j.jece.2021.105951>)
24. Y. Bulut, H. Aydın, *Desalination* **194** (2006) 259 (<https://doi.org/10.1016/j.desal.2005.10.032>)
25. K. Y. Foo, B. H. Hameed, *Desalin. Water Treat.* **19** (2012) 255 (<https://doi.org/10.5004/dwt.2010.1214>)
26. A. Sharma, N. Verma, A. Sharma, D. Deva, N. Sankararamakrishnan, *Chem. Eng. Sci.* **65** (2010) 3591 (<https://doi.org/10.1016/j.ces.2010.02.052>)
27. X. Shi, C. Wang, Y. Ma, H. Liu, S. Wu, Q. Shao, Z. He, L. Guo, T. Ding, Z. Guo, *Powder Technol.* **356** (2019) 726 (<https://doi.org/10.1016/j.powtec.2019.09.002>)
28. B. Gu, J. Schmitt, Z. Chen, L. Llang, J. F. McCarthy, *Environ. Sci. Technol.* **28** (1994) 38 (<https://doi.org/10.1021/es00050a007>)
29. L. Ding, B. Zou, W. Gao, Q. Liu, Z. Wang, Y. Guo, X. Wang, Y. Liu, *Colloids Surf. A* **446** (2014) 1 (<https://doi.org/10.1016/j.colsurfa.2014.01.030>)
30. C. Li, Z. Xiong, J. Zhang, C. Wu, *J. Chem. Eng. Data* **60** (2015) 3414 (<https://doi.org/10.1021/acs.jced.5b00692>)
31. T. S. Anirudhan, J. Nima, S. Sandeep, V. R. N. Ratheesh, *Chem. Eng. J.* **209** (2012) 362 (<https://doi.org/10.1016/j.cej.2012.07.129>)
32. M. A. Ahmad, N. A. Ahmad Puad, O. S. Bello, *Water Resour. Ind.* **6** (2014) 18 (<https://doi.org/10.1016/j.wri.2014.06.002>)
33. X. Zhou, J. Zhou, Y. Liu, J. Guo, J. Ren, F. Zhou, *Fuel* **233** (2018) 469 (<https://doi.org/10.1016/j.fuel.2018.06.075>).

SUPPLEMENTARY MATERIAL TO
**Performance of carbon-coated magnetic nanocomposite in
methylene blue and arsenate treatment from aqueous solution**

NGOC BICH NGUYEN^{1,2*}, THI QUE PHUONG PHAN³, CAO THANH TUNG PHAM^{1,4},
HUU NGHI NGUYEN², SY NGUYEN PHAM⁵ and DINH THANH NGUYEN^{1,3**}

¹Graduate University of Science and Technology, Viet Nam Academy of Science and Technology, Hanoi City, 100000, Vietnam; ²Dong Thap University, Cao Lanh City, 870000, Vietnam; ³Institute of Applied Materials Science, Viet Nam Academy of Science and Technology, Ho Chi Minh City, 700000, Vietnam; ⁴Institute of Chemical Technology, Viet Nam Academy of Science and Technology, Ho Chi Minh City, 700000, Vietnam and ⁵Ho Chi Minh City University of Natural Resources and Environment, Vietnam

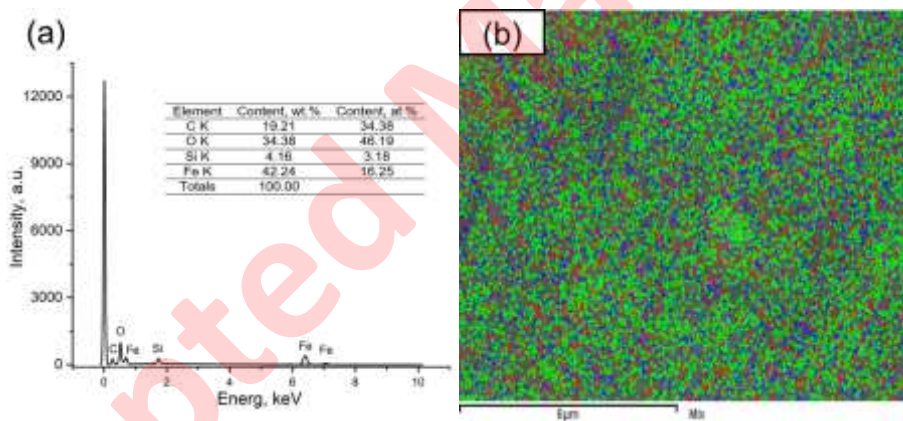


Fig. S-1. EDS analysis (a) and elemental map (b) of CMC

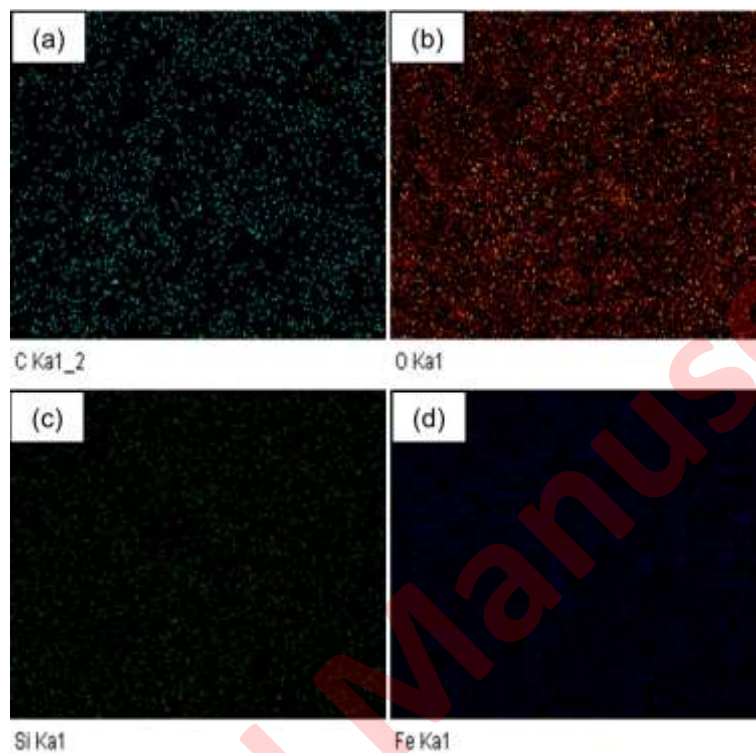


Fig. S-2. Elemental maps of C (a), O (b), Si (c) and Fe (d) of CMC

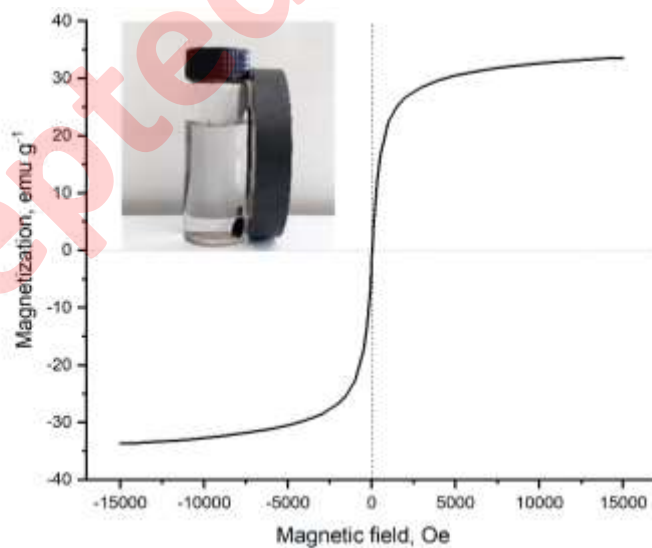


Fig. S-3. Magnetization curves and illustration of the magnetic separability of CMC

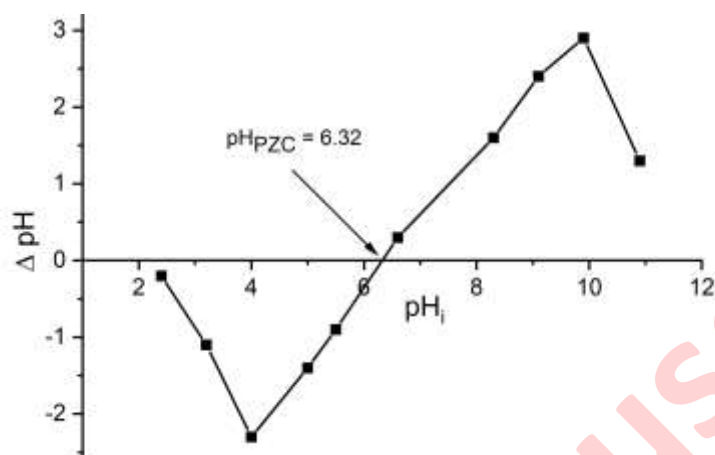


Fig. S-4. Plot of point of zero charge of CMC

TABLE S-I. Different kinetic models, thermodynamic equations and adsorption isotherms

Model	Parameter	Equation
Adsorption kinetic models		
Pseudo first-order	$q_e / \text{mg g}^{-1}$ = equilibrium adsorption capacity	$q_t = q_e - q_e e^{-k_1 t}$ (1)
	$q_t / \text{mg g}^{-1}$ = adsorption capacity at time t	
	k_1 / min^{-1} = rate constant	
Pseudo second-order	$k_2 / \text{g mg}^{-1} \text{min}^{-1}$ = rate constant	$q_t = \frac{k^2 q_e^2 t}{1 + k^2 q_e t}$ (2)
Thermodynamic equations		
	$\Delta S^\circ / \text{J mol}^{-1}$ = entropy change	$\ln K_D = \frac{\Delta H^\circ}{RT} + \frac{\Delta S^\circ}{R}$ (3)
Van't Hoff equation	$\Delta H^\circ / \text{J mol}^{-1}$ = enthalpy change	
	$R / \text{J mol}^{-1} \text{K}^{-1} = 8.314$ (universal gas constant)	
	T / K = absolute temperature	
	$K_D / \text{L g}^{-1} = q_e / C_e$	
	thermodynamic equilibrium constant	
	$\Delta G^\circ / \text{J mol}^{-1}$ = Gibbs free energy change	$\Delta G^\circ = -RT \ln K_D$ (4)
Adsorption isotherms		
Langmuir	$q_m / \text{mg g}^{-1}$ = maximum monolayer adsorption capacity of the adsorbent	$\frac{C_e}{q_e} = \frac{1}{K_a q_m} + \frac{C_e}{q_m}$ (5)
	K_a = energy constant	
	R_L = separation factor which gives an idea about Langmuir isotherm	$R_L = \frac{1}{1 + K_a C_0}$ (6)
Freundlich	$K_F / \text{mg g}^{-1} \text{L}^{1/n} \text{mg}^{-1/n}$ = Freundlich constant n = intensity of adsorption, $n > 1$ indicates a favourable and heterogeneous adsorption	$\ln q_e = \ln K_F + \frac{1}{n} \ln C_e$ (7)

TABLE S-II. The comparison of the magnetization of CMC with various biochar

Precursors of magnetic biochar	Method	Magnetization, emu g ⁻¹	Reference
Rice straw, Fe(NO ₃) ₃ , KOH	Hydrothermal	33.7	This work
Coconut shells, FeCl ₃	Pyrolysis, microwave	6.0	¹
Corn stalk, FeSO ₄ , Na ₂ S ₂ O ₃ , NaOH	Hydrothermal	11.2	²
Corn stalk, FeSO ₄ , Na ₂ S ₂ O ₃ , NaOH	Pyrolysis	20.4	²
Palm fiber, FeSO ₄ , FeCl ₃ , NH ₃	Pyrolysis	19.4	³
Firwood, α-FeOOH	Pyrolysis	20.8	⁴
Oleyl amine, FeCl ₂ , FeCl ₃ , NaOH	Hydrothermal	21.7	⁵
Rice husk, Fe(NO ₃) ₃ , KMnO ₄	Pyrolysis	27.5	⁶

TABLE S-III. The porous parameters of RS, BS, CMC samples

Sample	S _{BET} / m ² g ⁻¹	V _T / cm ³ g ⁻¹	D _p / nm
RS	1.3	0.01	30.6
BS	6.6	0.04	33.0
CMC	171.4	0.15	6.0

TABLE S-IV. The comparison of the maximum adsorption capacity of MB and As(V) on CMC with various adsorbents.

Adsorbent	Capacity, mg g ⁻¹		
	MB	As(V)	Ref.
CMC	110.63	2.31	This study
Fe ₂ O ₃ -ZrO ₂ /BC	38.1	1.01	⁷
M-MWCNTs	48.06	-	⁸
Fe ₃ O ₄ /MWCNT	74	-	⁹
Fe ₃ O ₄ @C NPs	117	-	¹⁰
HPB (hematite/biochar)	-	0.43	¹¹
Ch-Rs (chitosan/red scoria)	-	0.72	¹²
OBC (Canola straw-based biochar)	-	0.95	¹³
TB 800 (biochar from waste)	-	1.25	¹⁴
PAC-500 (magnetic biosorbents)	-	2.00	¹⁵
MC-O/NC-L-MG (magnetite/ microcellulose)	-	18.5	¹⁶
ChM (Chitosan-Magnetite Hydrogel)	-	66.9	¹⁷

REFERENCES

1. M. W. Yap, N. M. Mubarak, J. N. Sahu, E. C. Abdullah, *J. Ind. Eng. Chem.* **45** (2017) 287 (<https://doi.org/10.1016/j.jiec.2016.09.036>)
2. Y. Tu, Z. Peng, P. Xu, H. Lin, X. Wu, L. Yang, J. Huang, *Bioresources* **12** (2017) 1077 (<https://doi:10.15376/biores.12.1.1077-1089>)
3. X. Zhou, J. Zhou, Y. Liu, J. Guo, J. Ren, F. Zhou, *Fuel* **233** (2018) 469 (<https://doi.org/10.1016/j.fuel.2018.06.075>)
4. D. D. Sewu, H. N. Tran, G. Ohemeng-Boahen, S. H. Woo, *Sci. Total Environ.* **717** (2020) 137091 (<https://doi.org/10.1016/j.scitotenv.2020.137091>)
5. X. Bao, Z. Qiang, J.-H. Chang, W. Ben, J. Qu, *J. Environ. Sci.* **26** (2014) 962 ([https://doi.org/10.1016/S1001-0742\(13\)60485-4](https://doi.org/10.1016/S1001-0742(13)60485-4))

6. C. Sun, T. Chen, Q. Huang, J. Wang, S. Lu, J. Yan, *Environ. Sci. Pollut. Res. Int.* **26** (2019) 8902 (<https://doi.org/10.1007/s11356-019-04321-z>)
7. S. I. Siddiqui, S. A. Chaudhry, *J. Clean. Prod.* **223** (2019) 849 (<https://doi.org/10.1016/j.jclepro.2019.03.161>)
8. L. Ai, C. Zhang, F. Liao, Y. Wang, M. Li, L. Meng, J. Jiang, *J. Hazard. Mater.* **198** (2011) 282 (<https://doi.org/10.1016/j.jhazmat.2011.10.041>)
9. A. Suwattanamala, N. Bandis, K. Tedsree, C. Issro, *Mater. Today: Proc.* **4** (2017) 6567 (<https://doi.org/10.1016/j.matpr.2017.06.169>)
10. R. Wu, J.-H. Liu, L. Zhao, X. Zhang, J. Xie, B. Yu, X. Ma, S.-T. Yang, H. Wang, Y. Liu, *J. Environ. Chem. Eng.* **2** (2014) 907 (<https://doi.org/10.1016/j.jece.2014.02.005>)
11. S. Wang, B. Gao, A. R. Zimmerman, Y. Li, L. Ma, W. G. Harris, K. W. Migliaccio, *Bioresour. Technol.* **175** (2015) 391 (<https://doi.org/10.1016/j.biortech.2014.10.104>)
12. T. G. Asere, S. Mincke, J. De Clercq, K. Verbeken, D. A. Tessema, F. Fufa, C. V. Stevens, G. Du Laing, *Int. J. Environ. Res. Public Health* **14** (2017) 1 (<https://doi.org/10.3390/ijerph14080895>)
13. K. Zoroufchi Benis, J. Soltan, K. N. McPhedran, *Chem. Eng. J.* **423** (2021) 130061 (<https://doi.org/10.1016/j.cej.2021.130061>)
14. L. Verma, J. Singh, *J. Environ. Manage.* **248** (2019) 109235 (<https://doi.org/10.1016/j.jenvman.2019.07.006>)
15. L. Verma, M. A. Siddique, J. Singh, R. N. Bharagava, *J. Environ. Manage.* **250** (2019) 109452 (<https://doi.org/10.1016/j.jenvman.2019.109452>)
16. K. Taleb, J. Markovski, Z. Veličković, J. Rusmirović, M. Rančić, V. Pavlović, A. Marinković, *Arab. J. Chem.* **12** (2019) 4675 (<https://doi.org/10.1016/j.arabjc.2016.08.006>)
17. I. P. Verduzco-Navarro, E. Mendizabal, J. A. Rivera Mayorga, M. Renteria-Urquiza, A. Gonzalez-Alvarez, N. Rios-Donato, *Gels* **8** (2022) 1 (<https://doi.org/10.3390/gels8030186>)